Journal of Instrumentation

PAPER • OPEN ACCESS

Wideband precision stabilization of the -18.6kV retarding voltage for the KATRIN spectrometer

To cite this article: C. Rodenbeck *et al* 2022 *JINST* **17** P06003

Published by IOP Publishing for Sissa Medialab

Received: *March 28, 2022*
Accepted: *April 27, 2022*
Published: *June 6, 2022*

Wideband precision stabilization of the −18.6 kV retarding voltage for the KATRIN spectrometer

C. Rodenbeck,[a,*] S. Wüstling,[b] S. Enomoto,[c] J. Hartmann,[b] O. Rest,[a] T. Thümmler[d] and C. Weinheimer[a]

[a] *Institut für Kernphysik, Westfälische Wilhelms-Universität Münster, Wilhelm-Klemm-Str. 9, 48149 Münster, Germany*
[b] *Institute for Data Processing and Electronics (IPE), Karlsruhe Institute of Technology (KIT), Hermann-von-Helmholtz-Platz 1, 76344 Eggenstein-Leopoldshafen, Germany*
[c] *Center for Experimental Nuclear Physics and Astrophysics and Department of Physics, University of Washington Seattle, WA 98195, U.S.A.*
[d] *Institute for Astroparticle Physics (IAP), Karlsruhe Institute of Technology (KIT), Hermann-von-Helmholtz-Platz 1, 76344 Eggenstein-Leopoldshafen, Germany*

E-mail: rodenbeck@wwu.de

Abstract: The Karlsruhe Tritium Neutrino Experiment (KATRIN) measures the effective electron anti-neutrino mass with an unprecedented design sensitivity of 0.2 eV (90 % C.L.). In this experiment, the energy spectrum of beta electrons near the tritium decay endpoint is analyzed with a highly accurate spectrometer. To reach the KATRIN sensitivity target, the retarding voltage of this spectrometer must be stable to the ppm (1×10^{-6}) level and well known on various time scales (µs up to months), for values around −18.6 kV. A custom-designed high-voltage regulation system mitigates the impact of interference sources in the absence of a closed electric shield around the large spectrometer vessel. In this article, we describe the regulation system and its integration into the KATRIN setup. Independent monitoring methods demonstrate a stability within 2 ppm, exceeding KATRIN's specifications.

Keywords: Spectrometers; Voltage distributions; Neutrino detectors

ArXiv ePrint: 2203.13153

*Corresponding author.

https://doi.org/10.1088/1748-0221/17/06/P06003

2022 JINST 17 P06003

Contents

2022 JINST 17 P06003

1 Introduction

The Karlsruhe Tritium Neutrino (KATRIN) [1, 2] experiment is measuring the effective mass of the electron antineutrino with a targeted sensitivity of 0.2 eV/c^2 (at 90 % confidence level) within three live years of data taking. KATRIN examines the kinematics of tritium beta decays in a model-independent approach. The tritium beta-decay electron spectrum is measured near the endpoint at 18.6 keV, where the effect of the neutrino mass is the largest.

The experiment consists of a Windowless Gaseous Tritium Source (WGTS), a transport and pumping section [3], two spectrometers of MAC-E filter (Magnetic Adiabatic Collimation with an Electrostatic filter) type [4–6], and a focal plane detector [7]. The differential and cryogenic pumping sections prevent tritium gas inside the WGTS from entering the spectrometer. The

beta-decay electrons are magnetically guided to the spectrometers. A negative high voltage is applied to the main spectrometer vessel, creating a retarding potential for the electrons entering the spectrometer. Only electrons above a threshold energy can penetrate the potential to reach the detector. An energy spectrum of the electrons is recorded at the detector. The value of the retarding potential defines the energy scale for every electron spectrum.

Any high-voltage instability introduces a bias on the neutrino-mass measurement. To achieve KATRIN's physics goal, the standard deviation of any instability of the energy scale should be below 60 meV, corresponding to a stability requirement of 3 ppm (3×10^{-6}) at −18.6 kV on a wide range of time scales (µs up to months).

A measurement chain with two precision high-voltage dividers [8, 9] has been built and commissioned. It is combined with a custom-made, MHz-bandwidth regulation loop, called "post-regulation." The post-regulation stabilizes and sets the retarding voltage with the required precision.

The setup, its recent upgrade, and the performance of the post-regulation is presented in this paper.

2 Retarding high voltage at the KATRIN main spectrometer

The spectrometer is a large, barrel-shaped steel vacuum vessel with a maximum diameter of 9.8 m in its cylindrical section and a total length of 23.28 m [2]. Inside the main spectrometer, an electric field is created by a high voltage applied directly to the vessel itself. The electric field is fine-tuned with an inner electrode system consisting of full metal cones at the entrance and exit and two layers of wire grid electrodes in between. The inner electrode system is electrically biased by about −100 V (adjustable to the requirement of the measurements) relative to the spectrometer vessel (cf. [2], pp. 55 ff.). In the nominal symmetric configuration the maximum retarding potential qU for electrons of charge $q = -\mathrm{e}$ and the minimum electric field are in the central plane of the spectrometer. A superconducting magnet at each ends of the vessel and an air coil system create a guiding magnetic field. In the nominal configuration, the magnetic field has its minimum ($\approx 1 \times 10^{-4}$ T) at the central plane of the spectrometer and its maximum (4.2 T) at the entrance and exit of the spectrometer (cf. [2], pp. 66 ff.). The central plane, where the magnetic and electric field have their minimum, is called analyzing plane.

The transmission condition for beta electrons through the KATRIN main spectrometer depends on the magnetic field and electric potential settings and the potential of the WGTS tube, where the electrons are generated by tritium beta decay. The WGTS tube and the beam tube guiding the electrons to the main spectrometer are connected to the earth ground and serve as reference potential (cf. figure 1).

Electrons entering the spectrometer experience the Lorentz force by the electric and magnetic fields inside the spectrometer. In the adiabatic approximation, the magnetic field gradient keeps the orbital magnetic moment

$$\mu = \frac{E_\perp}{B} \tag{2.1}$$

constant (equation given in non-relativistic notation). Thus the magnetic field gradient collimates the electron momentum to be parallel to the magnetic field line in the center of the spectrometer, transforming the perpendicular or cyclotron component $E_\perp$ into the longitudinal component $E_\parallel$ of

2022 JINST 17 P06003

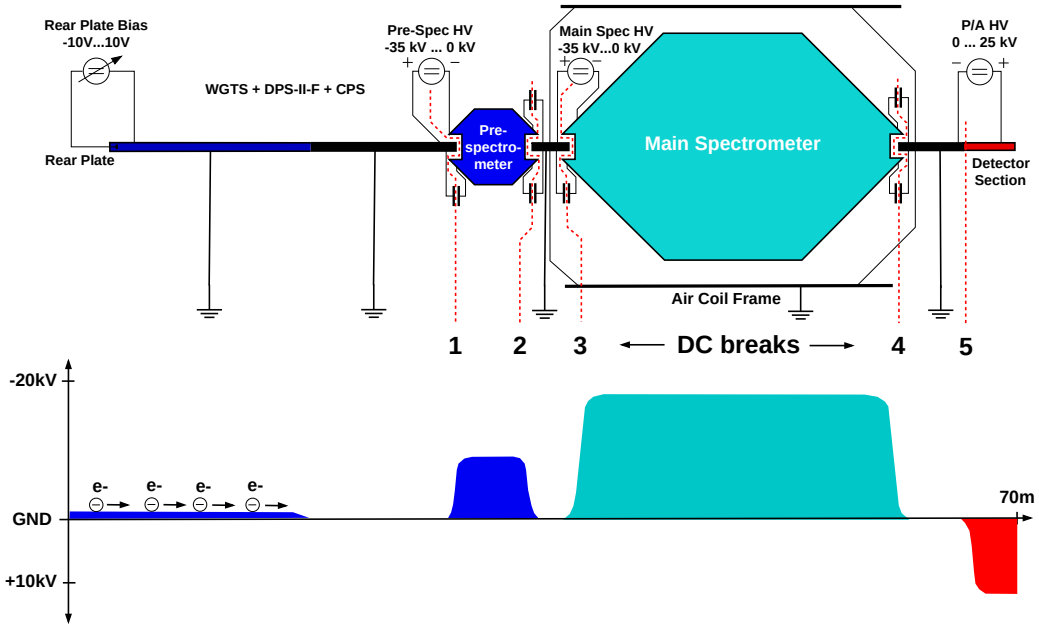

Figure 1. *Overall electrostatic potential scheme of the KATRIN experiment.* The upper plot shows the components of the KATRIN beamline, the lower one their electrostatic potential. On the left is the rear wall with an adjustable bias voltage. The bias voltage is used to optimize the plasma conditions inside the WGTS [10]. The plasma defines the starting potential of beta electrons in tritium source (WGTS). The WGTS and the transport and pumping section (DPS + CPS) are grounded. Both spectrometers can be set to different retarding potentials. The lower plot shows the nominal negative potential settings for the pre- and main spectrometer. Located on the right, after the 70 m beamline is the detector with a positive post-acceleration voltage. The red dashed lines mark the DC breaks. The main spectrometer potential shown in turquoise is the focus of this paper.

the kinetic energy. The electric field (cf. figure 2(a)) transforms the longitudinal component of the electrons' kinetic energy to potential energy on their way through the spectrometer. This is the MAC-E filter principle.

From the spectrometer entrance up to the analyzing plane of the spectrometer, the kinetic energy E_{kin} of the electrons is decreased. Their kinetic energy is increased again after the analyzing plane up to the spectrometer exit, if their kinetic energy is large enough to overcome the maximum retarding potential, otherwise they are reflected. Large enough kinetic energy means $E_{\mathrm{kin}} > qU_0$, for electrons with their momentum already parallel to the magnetiv field lines before entering the spectrometer (angle $\theta = 0$), with U_0 the retarding potential and q the charge of the electron. Therefore, the transmission function of electrons with $\theta = 0$ is a step from no transmission to full transmission at the threshold energy $E_{\mathrm{kin}} = qU_0$. For electrons with $\theta \neq 0$ the threshold energy is shifted towards higher values. These electrons need additional surplus energy to overcome the filter potential.

To quantify the effect on the transmission condition by a time-dependent noise on U_0, dedicated simulations were performed. In the following, the simulation results are used to define the requirements for the high-voltage stability. Possible sources for instabilities on different time scales are discussed.

2022 JINST 17 P06003

2.1 Requirements

To explain the general influence of high-voltage noise on electrons flying through the main spectrometer, a simplified model with on-axis electrons, and only their guiding motion is chosen. On-axis meaning that the electrons are following a field line along the spectrometer axis z ($x = y = 0$). We consider the electric potential $U(z)$ and the electric field $E(z)$ as the only z-dependent quantities.

The potential inside the spectrometer along the beam axis z can be described as $U(z) = a(z) \cdot U_0$. The z-dependence of the potential seen by the electron $a(z)$ is defined by the geometry of the spectrometer and can be determined with the Kassiopeia simulation framework [11]. With a time dependent fluctuating potential $\Delta U(t)$, the potential becomes:

$$U(z,t) = a(z) \cdot (U_0 + \Delta U(t)) = U(z) + a(z) \cdot \Delta U(t) \cdot \frac{U_0}{U_0} = U(z) \cdot \left(1 + \frac{\Delta U(t)}{U_0}\right). \tag{2.2}$$

The electric field is:

$$E(z) = -\frac{\partial U(t,z)}{\partial z} = -\frac{dU}{dz}\left(1 + \frac{\Delta U(t)}{U_0}\right). \tag{2.3}$$

Since the electric field (cf. figure 2(a)) is close to zero at the analyzing plane, it is virtually a Faraday cage. Here, any time-dependent variation, with $\Delta U(t) \ll U_0$ has only a small effect.

To investigate the effect of different noise waveforms, time-of-flight simulations were performed, building on previous work [12, 13]. In the simulation, the electrons are tracked in small steps along the z-axis inside the spectrometer. At each step their flight time and momentum are determined.

In figure 2(b), the electric field strength is plotted against the flight time of an electron through the spectrometer. Only the spectrometer entrance, where the electric field strength is largest is shown. The electron's travel time from the z-position, where the electric field starts to increase ($> 1\,\mathrm{V/m}$) to the z-position, where the electric field starts decreasing again to values below $100\,\mathrm{V/m}$, called t_{trav}, is within $1 \times 10^{-3}\,\mu\mathrm{s}$ to $0.1\,\mu\mathrm{s}$.

A sinusoidal noise $f_{\mathrm{sin}}(f,t) = A\sin(2\pi f t)$ on the retarding potential with a fixed amplitude A is used as test noise in the simulations. For frequency dependency investigations f was changed within 1 Hz to 1×10^9 Hz. For simplification only electrons with fixed angle $\theta = 0$ are considered here.

The result is shown in the left plot of figure 3. The noise broadens the transmission function by the height of the amplitude A, independent of the frequency for frequencies below 10 MHz. The independence of the frequency can be explained by t_{trav}. The change in amplitude of the noise $f_{\mathrm{sin}}(f,t)$ is slow, compared to t_{trav}. Only for frequencies above 10 MHz = 0.1 µs, the noise changes the electric field within t_{trav}. Therefore for frequencies below 10 MHz, the broadening effect of the sinusoidal test noise is the density distribution of $f_{\mathrm{sin}}(f,t)$, without any frequency dependency. For frequencies above 10 MHz the broadening effect on the transmission function starts to attenuate and vanishes for $f > 400$ MHz, see right plot in figure 3.

The broadening of the transmission function by a noise on the retarding potential directly shows the importance to eliminate its impact as much as possible, and to measure the residual broadening. Any unknown broadening of the energy scale, defined by the transmission function, leads to a shift of measured the neutrino mass by [14]

$$\delta m_\nu^2 = -2\sigma^2\,. \tag{2.4}$$

2022 JINST 17 P06003

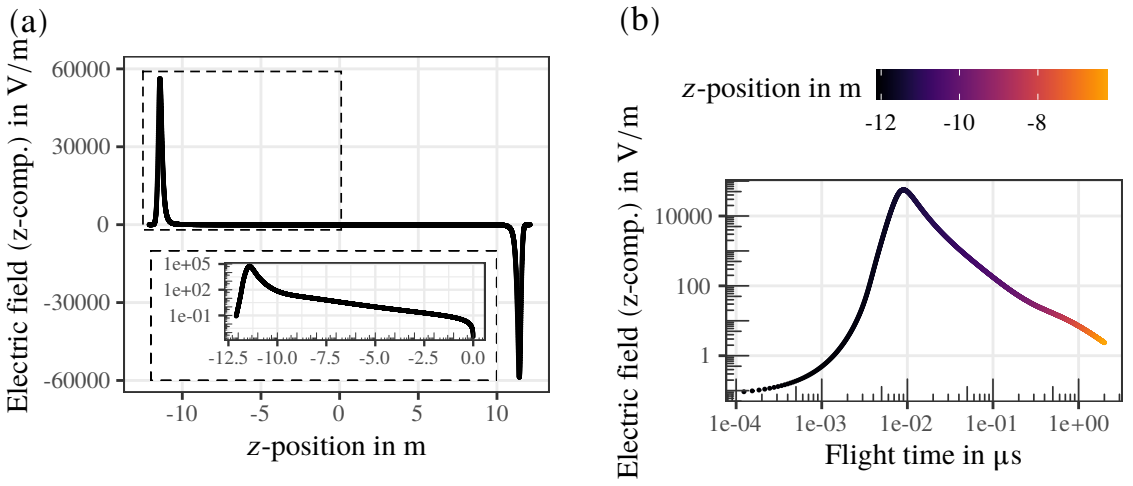

Figure 2. *Electric field.* Plot (a) shows the z component of the electric field along the beam axis z inside the main spectrometer ($z = 0$ center of the spectrometer). The retarding potential of $U_0 = -18\,500\,\mathrm{V}$ matches the standard measurement window below the tritium endpoint. Plot (b) shows the z component of the electric field plotted against the electron's flight time from the spectrometer entrance to a position along z. The flight time is calculated for an electron with a surplus energy of 0.5 eV and $\theta = 0$.

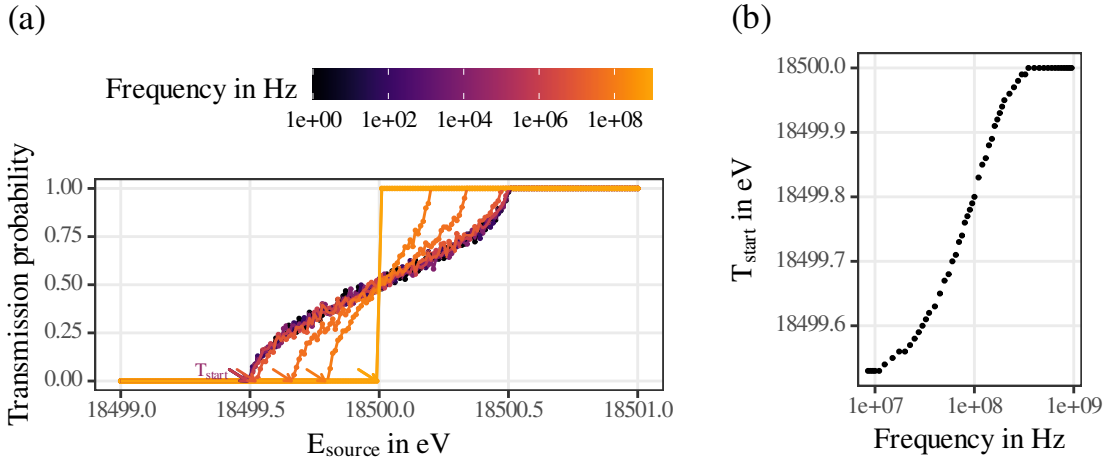

Figure 3. *Transmission conditions.* The left plot (a) shows the transmission function for electrons with $\theta = 0$ and different kinetic energies E_{source} at the spectrometer entrance. The retarding potential is fixed to $U_0 = -18\,500\,\mathrm{V}$ with a sinusoidal noise $f_{\sin}(f, t)$ with an amplitude of 0.5 V and at various frequencies f. For each frequency 100 000 electrons are generated. The start times are randomized with $t_{\mathrm{start}} \in [0, 1/f]$. The right plot (b) shows the minimal E_{source} for the transmission of the electron T_{start} (indicated with arrows in the left plot), as a function of the frequency.

2022 JINST 17 P06003

In the KATRIN design report [1], the uncertainty budget was specified to reach the design sensitivity. A neutrino mass shift of 7.5×10^{-3} eV was specified, leading to a maximum broadening of the energy scale of

$$\sigma = 60\,\text{meV}\,. \tag{2.5}$$

This is equivalent to an unknown Gaussian broadening of the retarding potential with a maximal standard deviation of 60 mV on all time scales: from the length of one measurement campaign (roughly 10 weeks [2]), down to 0.1 µs (10 MHz).

2.2 Short-term precision in a noisy environment

Apart from residual voltage ripple that may originate from the high voltage supply, the stability of the retarding voltage of the KATRIN main spectrometer can be compromised by external interference through electromagnetic coupling. An ideal countermeasure against such interference would be to place the spectrometer vessel in an overall electric shielding i.e. a Faraday cage. However, this would be impractical for the KATRIN apparatus. The strong capacitive coupling of the inner electrodes and the tank vessel prevents its use as a high-frequency shielding for the inner electrodes in view of the low noise requirement equation (2.5). As a consequence, any alternating electromagnetic fields in the vicinity of the spectrometer vessel represent possible interference sources for the retarding voltage. Alternating stray electric fields arise, for example, from AC power lines or radio transmitters. Moreover, there is an own floating 3-phase 400 V AC power network attached to the vessel, which is fed by a large insulation transformer with a 3×6 kV A rating. This floating AC supply is required mainly for the vacuum pumps (cf. [2], pp. 50 ff.) but also for various data acquisition and monitoring purposes. Although this transformer employs primary and secondary shield windings, there is a remaining capacitive coupling bringing about certain mains voltage interferences. Also, the large-area grounding network is sensitive to electromagnetic resonant pickups with possible effects on the retarding voltage. To achieve short-term precision of the retarding voltage, excessive high-frequency components need to be absent. As soon as high-frequency signals present in geometrically large apparatus are discussed, it is essential to specify *at which position* on the apparatus the high-frequency voltage component is most detrimental. Concerning the KATRIN main spectrometer, providing a smooth retarding potential within the spectrometer volume can be established by restoring a Faraday cage configuration of the beam tube, while DC voltage breakpoints (isolators) are present at the spectrometer entrances and exits. Especially at the electrical isolator, located at the spectrometer entrance, any noise must be reduced below a tolerable value (cf. section 2.1).

2.3 Long-term precision and absolute accuracy

A precision measurement chain is in place [1] to cover the requirements on the longer time scales. It consists of two custom-built precision high voltage dividers K35 [8] and K65 [9] and 8.5-digit precision digital voltmeters.[1] During measurements at the KATRIN beamline, one of the dividers is connected to the inner electrode system at the electrode providing the highest retarding energy qU_0 and thus defining the analyzing plane of the spectrometer. The 1972:1 tap of the K35 leads to

[1] Fluke 8508A.

2022 JINST 17 P06003

a reading in the 10 V range when operated at the nominal KATRIN standard measurement window around $U_0 = -18\,500$ V. The same is true for the K65 divider, which provides a 1818:1 tap.

Voltage measurements with sub-ppm accuracy [15] in the range of ±20 V can be achieved by using a voltmeter with high precision and regular calibrations to achieve trueness. The voltmeters are calibrated two times per week during measurement campaigns with multiple 10 V reference standards.[2] A subset of the reference standards is calibrated annually using a Josephson standard [2]. During regular measurements, the voltmeter readout rate is at 0.5 samples per second.

The dividers are calibrated regularly with independent methods. One method is an absolute calibration method [16], while the others involve spectroscopic measurements of mono-energetic conversion electrons from ^{83m}Kr electron capture decays [17]. Both methods are performed on-site and give matching results. They are also in agreement with cross calibration measurements at the Physikalisch-Technische Bundesanstalt (PTB) [8, 9]. The calibration history of both dividers, covering more than ten years, shows an excellent long-term stability to better than the ppm-level over a year [17].

This unique combination of precision high voltage dividers and voltmeters with regular calibrations and independent calibration methods achieves a robust measurement of the retarding potential on the sub-ppm level on time scales from 2 s up to years.

3 Motivation for a custom-designed high voltage system

As outlined in section 2.1, the requirements for retarding voltage not only imply an ultra-high stability over long time scales but also a low ripple up to frequencies in the MHz range. At the same time, the high-voltage generation system has to cope with a multitude of interference sources. To cover the long-term requirements, world-leading DC voltage measurement technology is being employed as shown in section 2.3. The design and implementation of the high-voltage generating system involved investigations of the suitability of commercially available power supplies to meet KATRIN's stringent technical and scientific requirements. Typically, commercial power supplies for the voltage range of interest (up to −35 kV) and the required power (several mA to drive voltage dividers, etc.) are switched-mode devices that operate at switching frequencies of some tens of kHz. They are available with ppm DC stability. However, the voltage regulation behaviour of these switched-mode supplies is quite slow. A principal limit to their regulation speed is given by the switched-mode principle. In practice, the regulation loop has to be even slower due to the loop stability requirements considering the slow speed of their multiplier cascade. There is a gap between what precision high-voltage DC metrology in combination with a commercial high voltage power supply can do and the high voltage stability requirements of the KATRIN experiment. Bridging this gap calls for a high-voltage system that allows low high-voltage source impedance for frequencies up to the MHz range.

Another important requirement for the high-voltage supply system to be designed is its output range. For neutrino mass measurements the retarding potential is varied around the endpoint at −18.6 kV in different step sizes from 1 V up to 200 V [18]. For systematic measurements the retarding potential is also needed at other values; for example the krypton conversion electron

[2] Fluke 732B.

2022 JINST 17 P06003

spectroscopy of ^{83m}Kr [19] requires the range of −32 kV to −7 kV. Not only is that voltage range different but also the scanning strategy. For ^{83m}Kr spectroscopy the voltage is changed often (about every 20 s to 180 s) in very small steps of 30 mV up to steps of 10 V, whereas the change frequency for tritium measurements is less frequently (varying roughly between 30 s to 20 min) in larger steps of around 2 V up to 300 V. Any voltage changes require additional settling times. To make measurements as efficient as possible the settling time needs to be minimized.

4 Implementation of the high voltage system

Typically one would use electric capacitors, to create a low impedance for AC voltages, while at the same time maintaining isolation for a high DC voltage. However, at the required low impedance values and capacitor voltage ratings, passive capacitive filtering is only viable above about 500 kHz. Considering frequencies such as the 50 Hz power grid frequency, unrealistically large capacitors, storing large amounts of energy and being a safety hazard, would be needed to reduce the overall interference level of the KATRIN main spectrometer.

Another method to obtain the same effect is to use an active voltage regulator. It consists of a precise pickup of the voltage present between the respective electric nodes, an adjustable precision voltage source for the setpoint, an error amplifier, a PID regulator, and an actuator that can control the voltage between the nodes. If a fast regulator action is required, all these components must be reasonably fast and exhibit low time delays. As outlined earlier, commercial HV power supply units do contain a voltage regulator, but it does not cover the required bandwidth into the MHz range.

The solution is a nested regulation approach. The primary high-voltage generation is provided by a commercial switched-mode high voltage power supply, which provides a good efficiency over a wide output voltage range. A second, linear regulation loop with a control range of only a few volts provides speed and fine regulation. Pick-up of the actual voltage is performed directly at the load for a maximum bandwidth. In our case, pick-up of the momentary retarding voltage is performed directly across the beam tube insulator at the main spectrometer entrance. To provide a low AC impedance even above the regulator upper cutoff frequency, ceramic filtering capacitors are arranged also at the beam tube insulator at the spectrometer entrance.

4.1 Philosophy of the regulator structure

To obtain a high-precision high-bandwidth readout and regulation of the actual voltage, a three-path scheme is employed. Smoothing is obtained by an AC-coupled control loop while DC regulation is obtained by a DC-coupled loop. The primary DC loop does not need to fulfill the full long-term high voltage stability requirements because the precision voltage divider along with its voltmeter readout (cf. section 2.3) can be integrated into the system by a secondary, software-based DC drift correction loop (figure 4).

The unwanted AC components are very small compared to the high voltage DC component. A precise observation of these AC components can be done through a high-voltage coupling capacitor that removes the DC component from the high-voltage signal. The remaining AC component can then be looked at without any attenuation, as opposed to using a frequency-compensated voltage divider serving both DC and AC stabilization. The absence of attenuation corresponds to a lower noise in the AC signal path. The AC pick-up capacitor with its associated protection circuitry is

2022 JINST 17 P06003

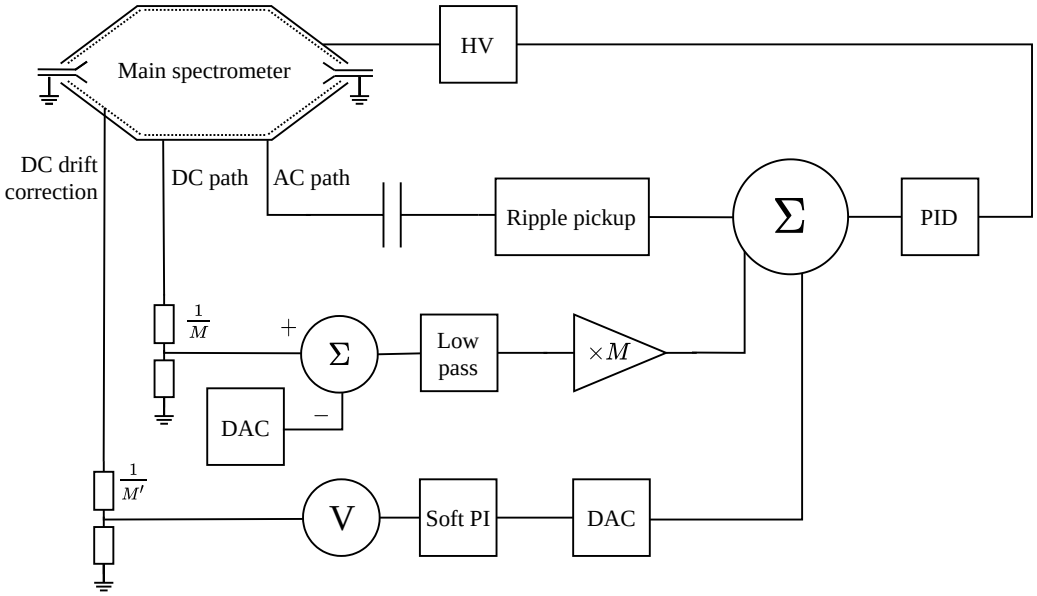

Figure 4. *Schematic diagram of the regulator structure*. The schematic shows the nested approach with the three paths: AC path, DC path, and the outer loop with the DC drift correction. The dashed line in the main spectrometer visualizes the inner electrode system (cf. section 2). A more detailed block diagram is shown in figure 7.

dubbed the "high-voltage ripple probe" in this context. A "ripple-probe amplifier" is connected to the high voltage ripple probe. A high dynamic input impedance of this amplifier provides a cutoff frequency of the AC pickup system at below 1 Hz. In this way, most of the regulator feedback loop bandwidth is covered by the low-noise AC path, resulting in a low total noise of the regulator.

An important design aspect is the required long-term precision of the DC loop. As outlined in section 2.3, there is already a precision voltage divider and a precision voltmeter that can provide precision high-voltage readouts every few seconds. Trying to obtain a similar long-term precision for the regulator DC stability would have amounted to duplicating the performance of the very expensive and sophisticated devices above, with very stringent stability requirements. However, there would be no added value to this effort: as soon the regulator DC pickup system offers a stability that fulfills the retarding voltage precision requirements for a few seconds, the high-precision readouts can be used to apply drift-compensating setpoint corrections of the DC loop. The DC loop medium-precision divider will be called the "auxiliary divider" below. Intuitively, one might wonder the feasability of using precision divider output also for the high voltage post-regulation DC component acquisition. However, there are several reasons, for keeping these signal paths separate:

- The circuit topology of the auxiliary DC pickup voltage divider input can be favorably made different from the conventional voltage divider topology. It can be combined with the associated input amplifier in an inverting configuration that maps the negative 0 kV to −35 kV HV range into a 0 V to 5 V range, very suitable for analog small signal processing.
- The validated precision divider system along with its precision multimeter should not be potentially compromised by connecting extra amplifiers and other auxiliary components.

2022 JINST 17 P06003

- The precision divider system has to be calibrated regularly. As long as the retarding-voltage regulation has its own divider, it remains operative, albeit with reduced long-term stability. The reduced long-term stability is sufficient for systematic measurements, for example background measurements, that are less sensitive to the retarding potential.

4.2 Shunt regulator principle and vacuum triode shunt device

A voltage-regulation method known for its fast and precise response is the so-called shunt regulator method. The load is fed from a roughly regulated voltage supply via a series resistor. The exact voltage across the load is adjusted by a controllable dump, or shunt, a device that takes over a part of the current coming from the primary voltage source across the series resistor. Such dump devices can be made to act quite fast. They are also very suitable for primarily capacitive loads, which applies to the KATRIN main spectrometer. If the shunt device is a controlled current source, the regulator loop stability will improve with increasing load capacitance — a property that not all voltage regulation principles have. Concerning the high voltage, shunt regulation was widely used to stabilize the CRT acceleration voltage in early color TVs in the late 1960s. The dump device in these units was a high-voltage vacuum shunt triode that would dump the full output power (some 35 W at 25 kV) of the high-voltage generator in case of a zero beam current (dark picture). Reusing these high-voltage triodes lends itself well for KATRIN high-voltage control as the tubes can still be purchased at a low price from the early color TV surplus stocks, and the voltage lies in the same range of around 25 kV. Using semiconductors would result in a complex stacking of multiple devices with the associated fast control circuitry and the components were much more susceptible to electrical transients. To assess the usability of these tubes, one must make sure that the maximum total interference current is lower than the maximum anode current of this tube type. For this purpose, the vessel was connected to earth ground via a 1 kΩ resistor and the AC current flowing through that resistor was measured. This measurement was made with the main electrical installations of the building and those on the vessel itself, powered through their insulation transformer, in place and running. The voltage signal across this resistor was measured using an oscilloscope. The overall peak-to-peak current amplitude was determined to be within 200 µA to 300 µA with a dominant 50-Hz sinusoidal from the stray fields of the power grid. This is well below the AC current component that can be compensated when running the shunt triode at a 0.7 mA anode current, which will keep the anode dissipation below 30 W even at 35 kV. If a peak value of 300 µA is assumed for the interference current, there will be a ±400 µA current control range left for other error sources, such as an output voltage drift of the primary (commercial) high-voltage power supply. The remaining control range for voltage deviations is given by multiplying this current range with the series resistor value. The series resistor connected between the primary high voltage power supply and the shunt triode in this system is a 22 kΩ device. The usable voltage control range of the post-regulation is therefore ±8.8 V.

Figures 5 and 6 show the triode shunt unit.

4.3 Acquisition of the actual high voltage value

As outlined in section 4.1, the acquisition of the actual, momentary high-voltage value is split into an AC path and a DC path, which will be described in the following. The high-voltage system in more detail is shown in figure 7.

2022 JINST 17 P06003

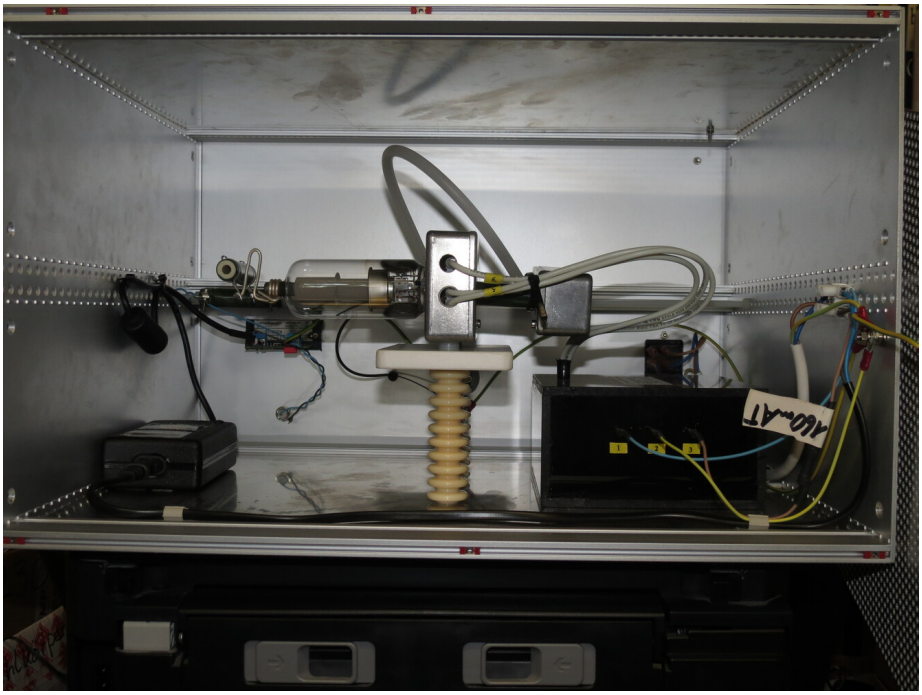

Figure 5. *View into the* 19″ *rack-mount enclosure of the shunt triode unit.* The anode cap of the Philips PD510 triode (on the left) is connected to the ground via surge limiting resistors. The cathode and grid side along with its fiber-optic-controlled circuitry is floating on the high voltage potential (center). Cathode heating and power supply for the control circuit is provided by an insulation transformer (on the right).

Figure 6. *Front side of the shunt triode unit.* The anode current can be read out visually via the LCD meter and electrically via a BNC receptacle.

2022 JINST 17 P06003

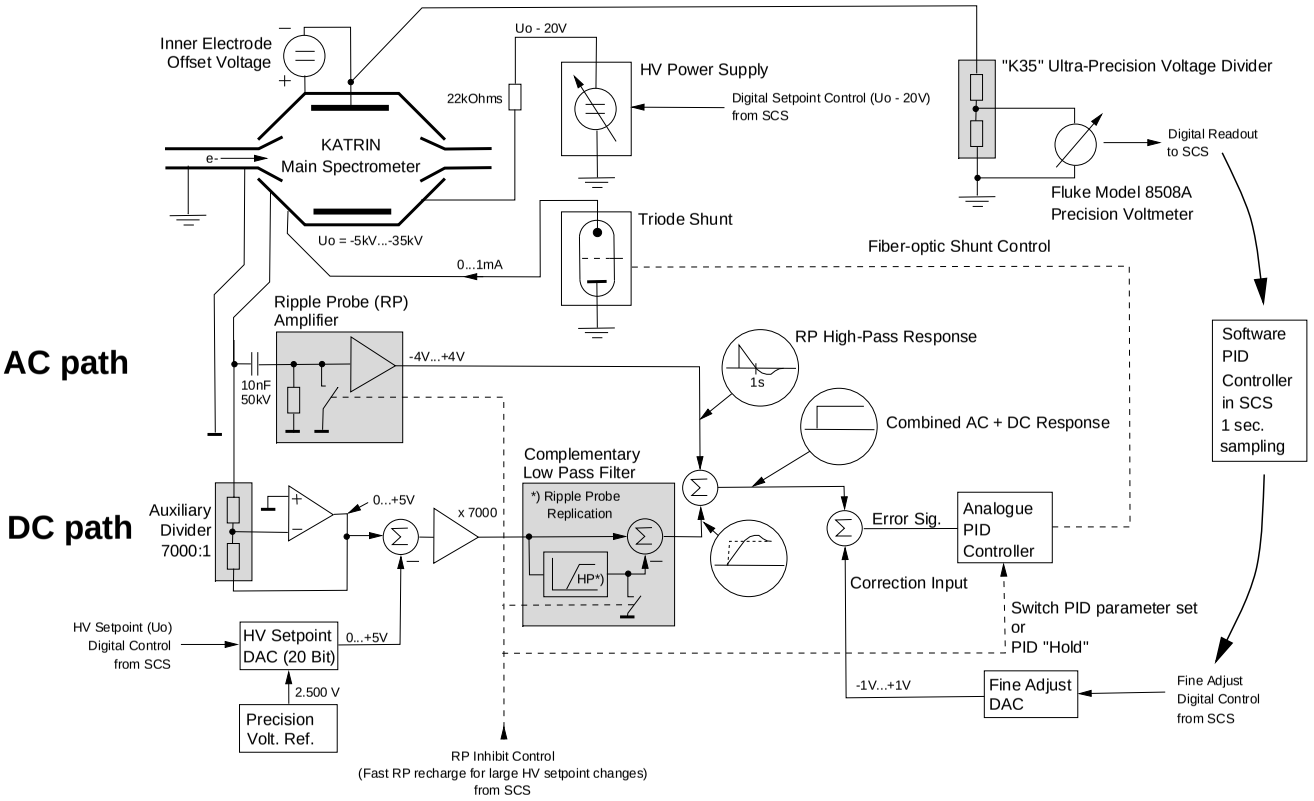

Figure 7. *Block diagram of the post-regulation system.* A detailed block diagram of the post-regulation setup at KATRIN's main spectrometer.

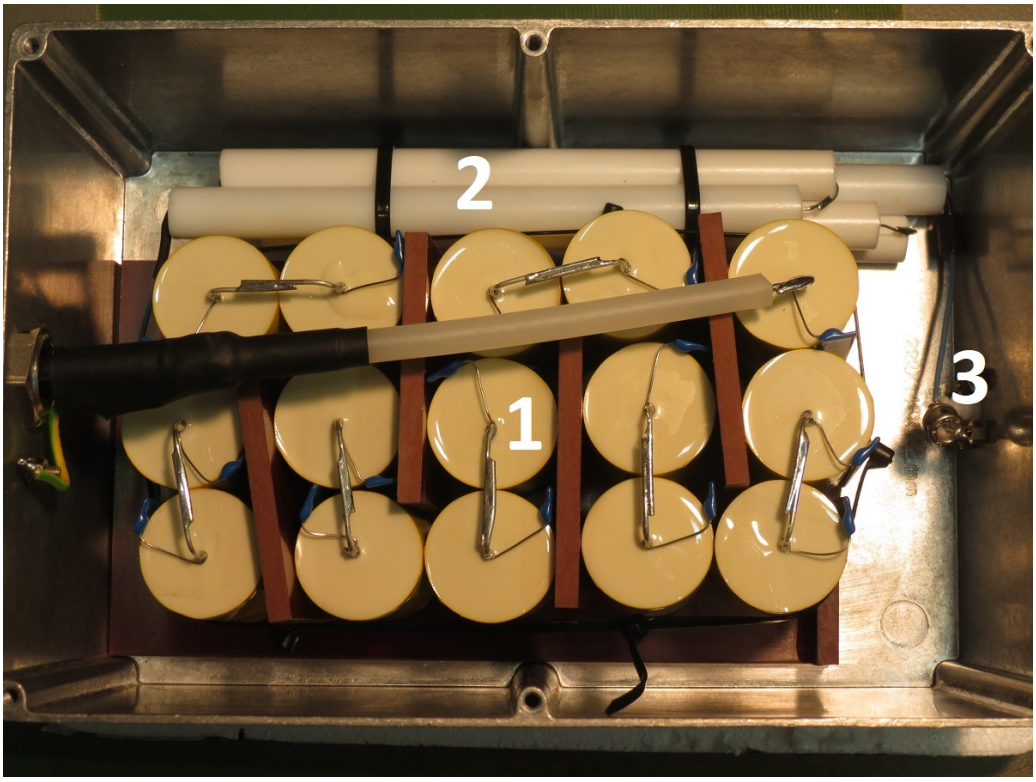

Figure 8. *Picture showing the interior of the ripple pick-up probe.* The device consists of 15 series-connected 150 nF / 3 kV foil capacitors with balancing resistors (1), a surge protection resistor chain (2), and a gas discharge surge arrester (3). All components are embedded in silicone potting that has not been applied in this photo yet. The width of the enclosure is about 21 cm.

4.3.1 AC path

The central element of the AC path is the high-voltage decoupling capacitor that separates the ripple pickup amplifier from the DC component of the high voltage. This capacitor must be of very high quality, partial discharges must be absent at a level of ppm or below. In KATRIN, a series connection of 15 150-nF foil capacitors is used, after experiments of high-voltage capacitors with paper/oil or ceramic dielectric showed significant partial discharges. Balancing of the foil capacitor chain is done with 15 resistors of 1 GΩ each. Figure 8 shows the interior of the "ripple probe" before the potting with an elastic, transparent silicone compound.

The ripple pickup amplifier has a very high dynamic input impedance (30 MΩ), obtained by a bootstrap scheme. This method provides a high dynamic input impedance while at the same time being able to compensate for constant DC leakage currents up to several µA.

With the balanced chain of capacitors, this leakage current is mainly given by the balancing resistor current. Another required property of the ripple pickup amplifier is the ability to withstand high-energy voltage transients at its input. The pickup capacitor represents a very low impedance for sharp voltage transients. Such transients can easily occur due to sparking, which may happen somewhere in the large spectrometer apparatus due to bad insulation vacua and similar during commissioning A multi-stage protection scheme is employed at the amplifier input, which consists

2022 JINST 17 P06003

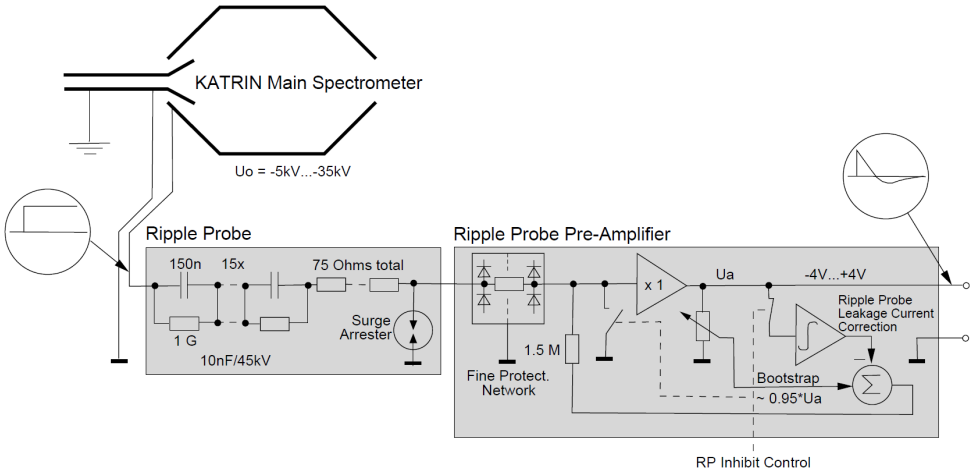

Figure 9. *Ripple pick-up circuitry.* Block diagram for the ripple probe and its pre-amplifier.

of a gas surge arrester and three stages of protection diodes with each stage installed in its shielding chamber. Decoupling resistors between the stages are chosen to be high enough to exhibit enough transient damping and low enough not to limit amplifier bandwidth.

The AC path of the post-regulation loop will counteract *any* changes in the output high voltage, which also applies for *intended* setpoint steps. This is why an inhibit feature was built into the AC path. If experimenters want to apply a high voltage setpoint step larger than the AC path measurement range ($\sim 4\,V_{pp}$), an inhibit signal can be asserted that blocks AC smoothing. This function will shorten the ripple amplifier input to ground, thus allowing the ripple pickup capacitor to quickly recharge to the new voltage. At the same time, the integrator of the leakage current compensation will be disconnected, which retains the leakage current status until the voltage has settled to the new value. However, this method requires corresponding actions in the remaining regulator loop to maintain stability. These provisions, such as the adjustment of the PID regulator parameters, are not yet fully implemented. This is why the experiment has not yet implemented the AC-path inhibit feature. The ripple amplifier protection circuitry will still allow for the ripple probe to recharge with an increased settling time.

The obtained overall settling times and other control-related properties are given in section 4.5 below.

4.3.2 DC path

The DC loop consists of an auxiliary, medium-precision voltage divider, a “zero offset” operational amplifier stage, a 20-Bit precision setpoint DAC with an ultra-low noise reference voltage source, and a subtraction stage. The output of the subtraction stage represents a DC error signal. The error signal is amplified by two further amplifier stages by a factor equal to the reciprocal of the voltage-divider ratio (7000x). Therefore, a 1 V change at the output of these stages corresponds to a 1 V change of the high voltage, similar to the output of the AC ripple pickup signal path. Ideally, the sum of the step response signals of the DC and AC pickup paths should form an ideal step response signal again. This is why the DC path is equipped with a special low-pass filter formed

2022 JINST 17 P06003

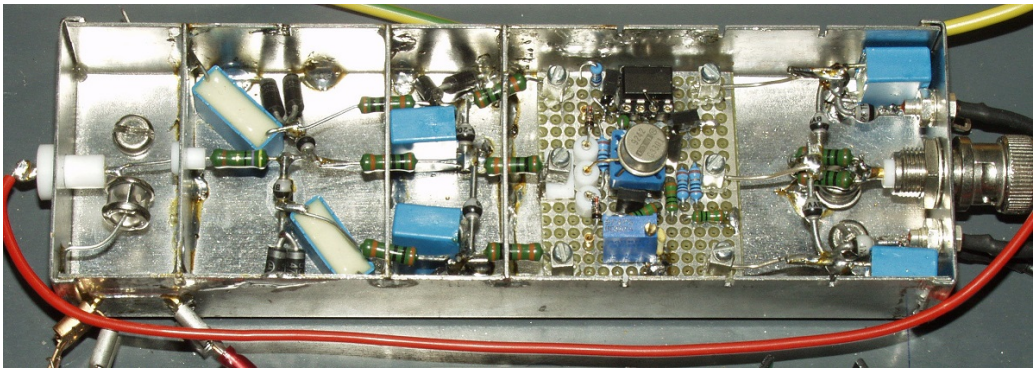

Figure 10. *Ripple pick-up amplifier with multi-stage transient protection.* The HV ripple probe is connected to the terminal on the left side. The RF-type enclosure is partitioned into several chambers to attenuate transient propagation. The chambers contain (left to right) surge arrester, stage 1 protection diodes, stage 2 protection diodes, stage 3 protection diodes, and the amplifier circuit.

by a high-pass filter and another subtraction stage. The high-pass filter consists of a replica of the AC path. Therefore, the overall DC path step response is complementary to that of the AC path. Figure 11 shows the auxiliary divider consisting of a helical resistor chain and two field-shaping discs. The design objective of this divider was to be able to hold the required KATRIN retarding voltage accuracy for about 10 s. This is — with some headroom — the time the precision HV readout (cf. section 2.3) needs to produce a valid measurement. The resistors used for the auxiliary divider are of the Caddock USF200 series. Each of these resistors consists of two individual resistor elements of opposite temperature coefficients, glued back to back.

4.4 Fast-stepping input and DC drift correction

After merging the outputs of the DC and AC pickup paths into the 1 V/V error signal, it is possible to add a "fast-stepping" analog control voltage before passing the error signal to the (PID) regulator. Using this input, it is not only possible to add an intentional wide-bandwidth waveform to the regulator setpoint, but this input also allows fine control of the high voltage beyond the resolution of the 20-bit setpoint DAC.

In the system presented in this paper, this input is used to overlay drift correction values derived from readouts of the precision voltage divider readouts as outlined in section 4.1. A software PI regulator reads the precision divider output via the precision voltmeter, and creates a correction input via a special fine-adjustment DAC, by comparing it with the HV setpoint from the experiment control. We use a 10-bit DAC from the experiment automation system that provides an output range of −10 V to 10 V. The DAC output voltage is fed to the post-regulation"fast-stepping" input through a 10:1 voltage divider and can therefore provide a fine-adjustment range of ±1 V.

4.5 Dynamic setpoint control

For measurements done with the main spectrometer, the retarding potential needs to be changed synchronously with data taking at the detector. Therefore the control of the post-regulation is done in close connection with the data acquisition system for detector data. For most of the measurements (tritium spectrum spectroscopy, ^{83m}Kr conversion electron calibration measurements), the setpoint

2022 JINST 17 P06003

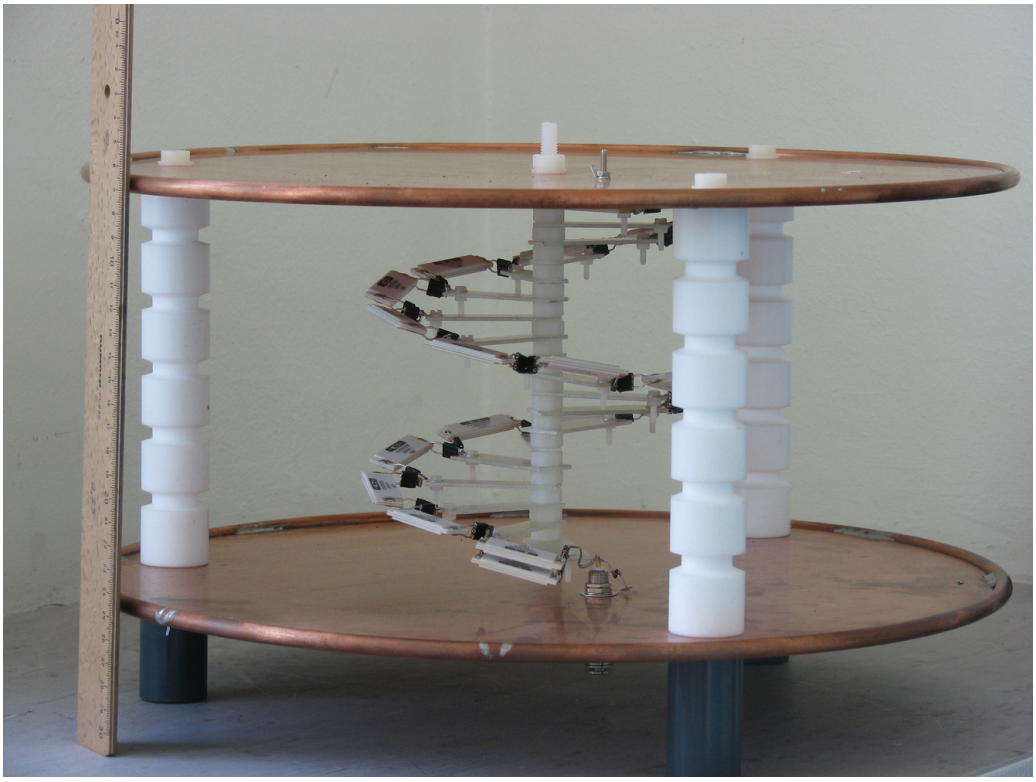

Figure 11. *Auxiliary voltage divider.* The helical resistor chain of the divider is located in between two field-shaping copper plates at the top and bottom.

of the retarding potential must not only be reached as fast as possible but also be stable and reproducible on the ppm-level [18].

The logic of setting a voltage value is set is shown in detail in figure 12. First, the voltage value is set coarsely $O(100\,\mathrm{mV})$. For this operation two inputs are needed. The setpoint for the primary high voltage supply needs to be more negative than the required spectrometer voltage to account for the voltage drop on the shunt regulator series resistor. This offset value c depends on the individual setup; i.e. how many and which dividers are connected to the main spectrometer and which power supply is used (as they can have varying absolute setpoint precision). The offset c needs to be chosen in a way, that the shunt triode is not overloaded (limited to 30 W), but still in its optimal working range of 0.5 mA to 0.9 mA. During the commissioning measurements, c is determined for each setup, depending on the voltage value and stored in a look-up table. The second input is the scale factor M of the auxiliary divider. For new voltage setpoints U_0, $M(U_0)$ is determined by values estimated during commissioning measurements and updated after each successful setting of the voltage.

After setting the voltage coarsely, the actual voltage is measured with one of the precision dividers. If necessary, M is adjusted, until the voltage value has reached its setpoint within $\pm 50\,\mathrm{mV}$. The DC drift correction is subsequently activated, regulating any remaining deviation and forcing the voltage to the desired U_0. Usually during data taking a loop that determines and stores the actual M continuously (not drawn in figure 12) is activated. For small voltages steps $< |50\,\mathrm{V}|$, the most recent value of M is used, instead of the $M(U_0)$ from the look-up table. For this step-size,

2022 JINST 17 P06003

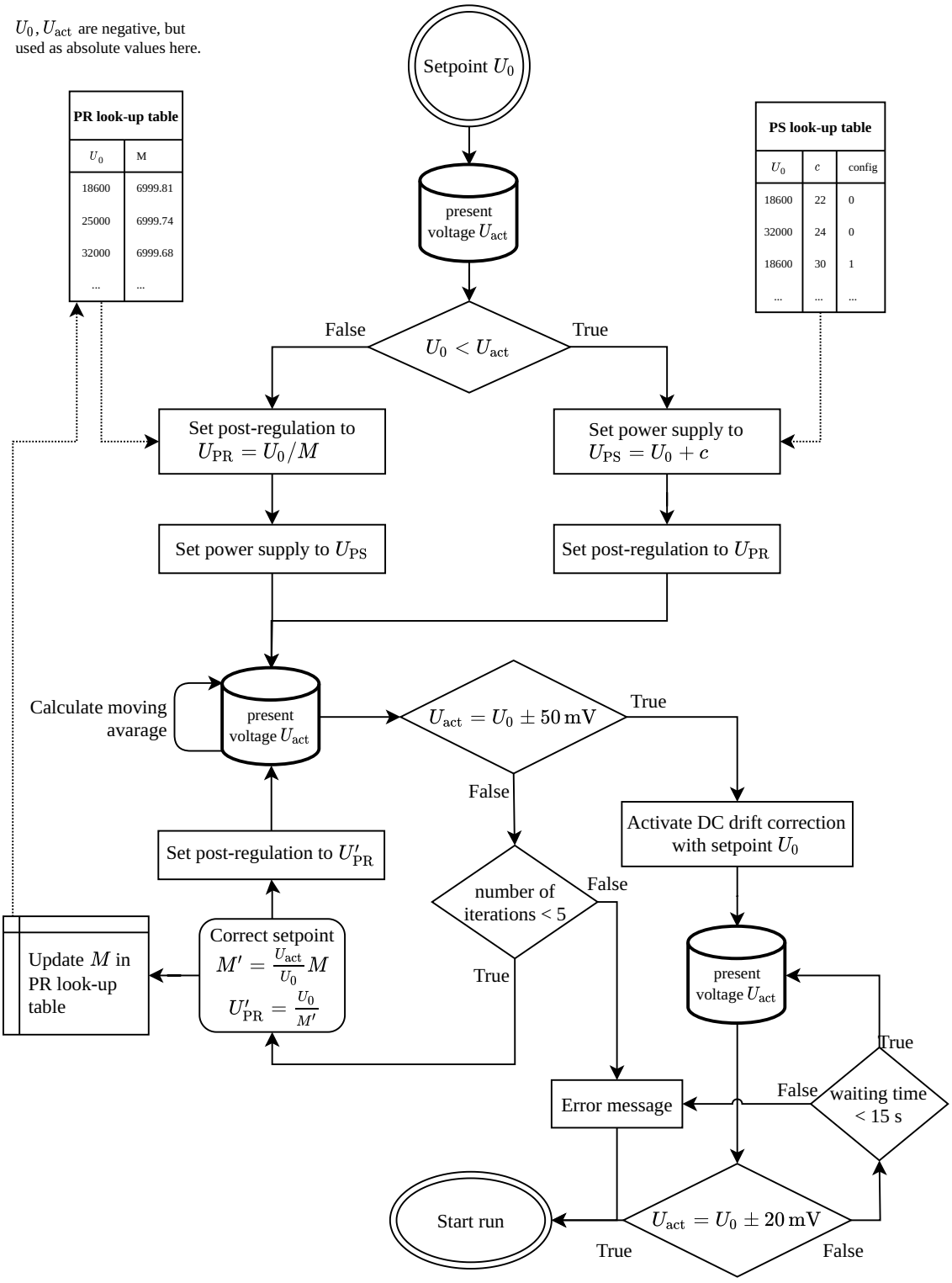

Figure 12. *Dynamic setpoint control.* Schematic of the logic for a new voltage setpoint. "Start run" means the start of data taking at the KATRIN beamline with a new voltage setpoint.

changes over time (mainly temperature related) have higher relevance than the voltage dependency of the auxiliary divider.

Due to the dynamic logic of the setpoint algorithm, the overall settling time for each voltage setpoint depends on the overall step size, the repetition of voltage steps, and especially the required precision. For ^{83m}Kr measurements it takes on average 22 s to 25 s, depending on the step size; the smaller the overall step size, the longer the average settling time. For standard tritium beta scans, the average step size takes 29 s on average and is larger than for ^{83m}Kr measurements. One dominant factor of the settling time is the averaging time over multiple measurements to ensure the setpoint precision before starting a physics measurement. During these measurements, data is taken continuously at the detector, but separated into "usable" periods with start/stop time stamps. In the analysis, this time can be recovered again by using the measured voltage values to redefine the start/stop time of a physics measurement. With this analysis, the average settling time is reduced for beta scans to 23 s without losing any precision.

4.6 X-ray safety

The shunt triode operating at anode voltages of up to 35 kV is a source of stray X-ray radiation and is subject to radiation protection legislation. Appropriate shielding must be installed and official permission is required prior to operation. 35-keV X-rays are relatively soft and are very effectively shielded by the 2.5-mm stainless steel walls of the post-regulation electronics cabinet. The cabinet door is fitted with a switch that will cut the power to the shunt triode control and cathode heating when the door is opened. LED indicators of the post-regulation electronics and a cathode current meter can be read through lead glass windows installed in the cabinet door. After a review of the cabinet and radiation measurements by an authorized radiation safety engineer, a permit was issued by the authority, Regierungspräsidium Karlsruhe.

5 Performance measurements

During the development of the post-regulation system, several quality and performance checks were carried out [20, 21]. At present four different methods allow for a measurement of the remaining ripple on the main spectrometer retarding voltage on different time scales. In this section, the performance of the final implementation, for the neutrino mass measurements, is evaluated with these methods.

5.1 Ripple pick-up probe

The ripple pick-up probe (cf. section 4.3.1) allows for a measurement of the AC noise on the retarding potential. Traces of the ripple pick-up probe at −18.3 kV are shown in figure 13. Without the post-regulation, the AC noise is dominated by a sinusoidal 50 Hz signal, with amplitudes of about 0.25 V. With the post-regulation active the sinusoidal noise is suppressed and only fluctuations within less than 0.03 V remain.

To analyze the AC components further, 100 traces at a sampling rate of 10 kHz are taken. Each trace was limited to 8192 samples. To remove any remaining DC part, the mean voltage value is first calculated for each trace, which is then subtracted from each voltage value within one trace. A fast Fourier transformation with a Hamming window (window function) is applied on the net

2022 JINST 17 P06003

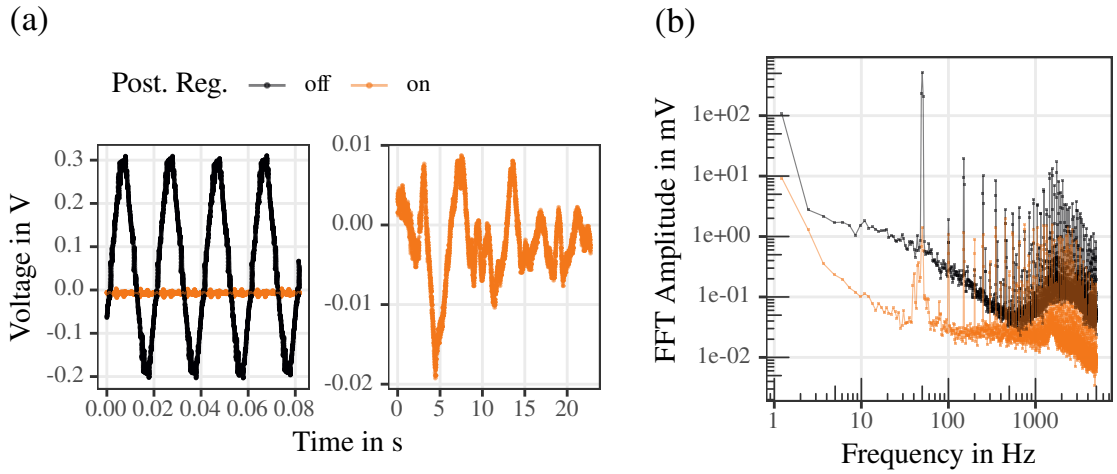

Figure 13. *Oscilloscope readout of ripple pick-up probe.* Two traces taken with the ripple pick-up probe at −18.3 kV main spectrometer potential are shown. In (a) a measurement without the post-regulation at a sample rate of 10 kHz and with active post-regulation at a sample rate of 250 Hz, is shown (please note the different scales). Plot (b) shows the Fourier spectrum for both cases.

trace and plotted in the right plot of figure 13. Comparing the Fourier spectrum with and without active post-regulation, one can see a noise reduction on a wide range of frequencies. The largest component at 50 Hz is suppressed by two orders of magnitude.

5.2 Conversion electron lines from ^{83m}Kr

Measurements with conversion electron lines from ^{83m}Kr provide an independent method to the ripple pick-up probe measurements. The conversion electrons from ^{83m}Kr are equally sensitive to the ripple as the beta decay electrons, whereas the ripple pick-up probe is only attached to the outside of the main spectrometer vessel. Therefore the electrons are an ideal tool for an independent cross-check of the post-regulation performance.

Measurements of ^{83m}Kr conversion electron lines are a standard method at KATRIN [17, 22, 23]. The measurements discussed here were performed with the *condensed Krypton source* (CKrS) during a measurement campaign described in [24]. They consist of measurements from three conversion electron lines, following the 32-keV gamma transition, but from different shells: K-32 at 17.8 keV, L_3-32 at 30.5 keV and the line doublet N_2N_3-32 at 32.1 keV.

For a typical transmission function scan of a conversion electron line with the main spectrometer, the retarding potential is changed in small steps (0.1 V to 0.5 V) around the expected line position. The width of the measured transmission function depends on the spectrometer resolution and the natural line width. Each transmission function has a retarding potential at which the rate is half of the rate compared to full transmission, called the middle of transmission. The rate in the transmission region is correlated with the retarding potential. For small variations of the retarding potential (< 1 V, depending on the width of the transmission function) around the middle of transmission, the measured electron rate at the detector is linearly dependent on the retarding potential.

By measuring the shape of the transmission function in a dedicated measurement the linear dependency of the rate on the retarding potential can be estimated. In a second step, the rate at the

2022 JINST 17 P06003

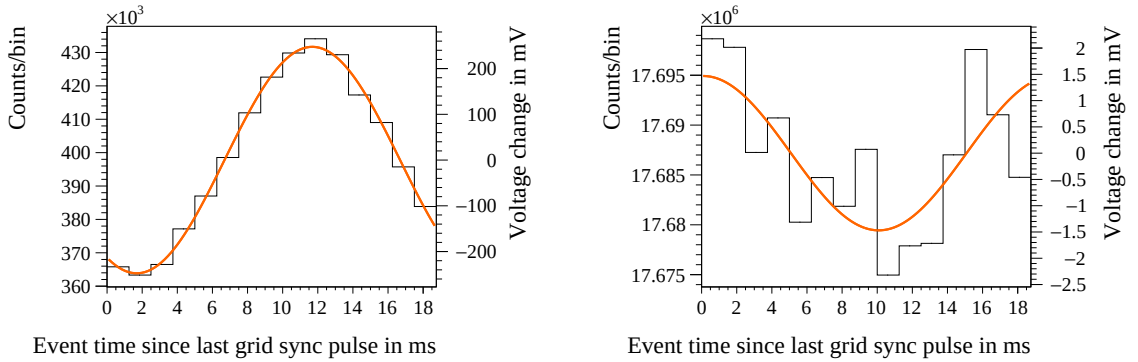

Figure 14. *Line-center measurements.* Results of the line-center measurement with the L_3-32 line. The left plot shows a 10.5-minute measurement without post-regulation. A clear sinusoidal ripple with an amplitude of 33 922(231) counts, transforming to a voltage ripple of 247(2) mV is visible. The 7.5-hour measurement with active post-regulation is shown in the right plot. Here the sinusoidal structure is not as significant. Still, a fit results in an amplitude of 7741(1592) counts transformed to a voltage ripple of 1.5(3) mV.

middle of transmission is measured. Assuming a perfectly stable source any fluctuations of the rate can then be accounted as fluctuations of the retarding potential.

The measurements focus on the largest noise part, coming from the 50 Hz power grid interference. The dedicated grid synchronization signal at KATRIN's focal plane detector (FPD) measures the ≈ 50 Hz frequency of the mains power and outputs a synchronization pulse (called the *grid sync pulse*) for each new mains power period (cf. p. 79, [2]). With this, each event measured at the FPD has a relative time to the start of a new mains power period t_{rel}.

Measuring the rate at the middle of transmission and stacking the measured events at the detector along t_{rel} modulo 20 ms reveals directly any 50 Hz noise seen by the electrons on their way through the spectrometer. In the following, this type of measurement is called the *line-center* method. The result of such a measurement is plotted in figure 14. The left plot is without post-regulation. Here the rate at the middle of transmission is following a 50 Hz sinusoidal ripple. In a dedicated transmission function scan, the slope around the middle of transmission is determined. With the slope, the rate change can be transformed to a voltage ripple of about 0.25 V. In the right plot, with active post-regulation, the sinusoidal structure is not as distinct, despite a 43-fold increased measurement time. This clearly shows the ability of the post-regulation to decrease the 50 Hz sinusoidal ripple by at least two orders of magnitude.

By repeating the line-center method at different line positions, a possible dependency on the size of the retarding potential can be investigated. It also allows the comparison of the measured ripple amplitude at the ripple probe to the amplitude measured by the line-center method. To investigate the sensitivity of the method, measurements with different power supplies and without post-regulation were performed.

Without post-regulation the ripple amplitudes as measured with the ripple probe and the line-center method are in good agreement, see results in table 1. The only exception is the measurement with power supply B. Here the deviation between both methods is larger than for devices A and C but most likely due to a drift of the device between the ripple probe and the line-center measurement. This device was added to the measurements to have a larger variety of devices but is not used

2022 JINST 17 P06003

Table 1. *Ripple amplitudes without post-regulation.* The amplitudes are estimated by two different measurement methods (line-center and ripple probe), for different power supplies. The ripple amplitude as measured with ^{83m}Kr conversion electrons at the detector (line-center) and of the ripple probe is determined by fitting a sinusoidal with free amplitude.

Line	Ret. pot (kV)	Power supply	Ripple probe (mV)	Line-center (mV)
K-32	−17.8	A	225(1)	219(4)
		B	234(1)	222(4)
		C	210(1)	204(4)
L_3-32	−30.5	A	248(1)	246(2)
		B	258(1)	248(2)
		C	229(1)	231(2)
N_2N_3	−32.1	C	233(1)	237(6)

in normal measurement campaigns, due to its increased instabilities and fluctuations compared to devices of the same type. Note that any drift of the power supply would be compensated by the post-regulation within its regulation limit (cf. section 4.2).

The variety of tests show that the ripple probe measurement and the line-center method yield very similar results for the amplitude of the 50 Hz noise. This proves, at least for the 50 Hz noise, that the ripple probe readout matches the ripple seen by the electrons inside the main spectrometer.

With post-regulation, the comparison of both methods is more difficult, since here the sinusoidal 50 Hz noise is not the dominant part (cf. figure 13) and the line-center method is only sensitive to the 50 Hz. Still, both methods show the clear mitigation of the 50 Hz ripple by the post-regulation.

5.3 Precision high voltage divider

As described in section 2.3, a continuous measurement of the retarding potential with a readout rate of 0.5 Hz of a precision high voltage divider is in place. The stability of an exemplary one-hour measurement at a fixed retarding potential of −18.6 kV is shown in figure 15. Without the DC drift correction a random-walk-like structure within ±3 ppm is visible. With active DC drift correction, the measured voltage has a standard deviation of 11 mV. This Gaussian-like distribution is valid at all times from minutes to two weeks. It is only limited by the long-term stability of the divider and voltmeter.

To cover the gap in frequency between the sensitivity range of the high voltage divider and the ripple probe measurement, an additional measurement system, the “fast-measurement system”, was temporarily installed [21].

The fast-measurement system measures the vessel potential as a difference voltage to a reference potential. The reference potential is supplied by a sufficiently stable power supply[3]. For instance, when aiming for a measurement in the range of −18 600 V, the reference potential is set to a value close to this voltage (e.g. −18 590 V), such that the difference voltage is in the order of 10 V. This voltage range can be measured directly with a voltmeter, without a high-voltage divider inbetween.

[3]The power supply used for this setup is a FuG HCP 70M-35000. Its stability is verified to be 2 ppm over 8 h [21].

2022 JINST 17 P06003

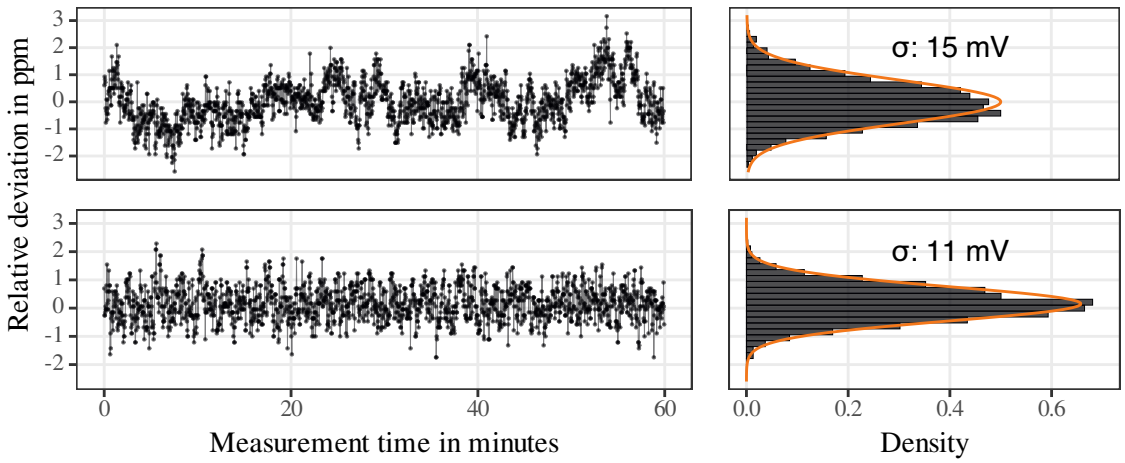

Figure 15. *Stability measurements.* Measurement with the precision high voltage divider K35 over 1 h at a retarding potential of −18.6 kV. The upper plot shows the performance without the DC drift correction, the lower with the DC precision loop active.

Therefore a 6.5-digit measurement offers a more than sufficent precision (mV resolution is sufficient) and allowing a fast and precise measurement, with a sample rate of 3 Hz.[4] The reference potential is monitored with a high voltage divider, scaling the reference potential down by a factor of about 2000 and measuring it with 8.5-digit precision at a readout rate of 1/4 Hz. In the analysis, the vessel potential is then estimated by adding the difference voltage to an interpolated value of the reference potential.

One exemplary measurement over 20 min is shown in figure 16. During the measurement, the DC drift correction was not used. The relative deviation over time is similar to the one measured with the standard measurement setup (upper plot in figure 15); the voltage is changing randomly within ±3 ppm.

5.4 Evaluation over the full frequency range

As presented above with all three methods: high-voltage divider, fast-measurement system and ripple probe, the stability of the retarding potential was investigated at a fixed value of −18.6 kV. To evaluate the stability on different time scales even further, the Allan variance method [25] is used.

The Allan variance provides a tool to estimate the stability of a sensor due to noise sources on all time scales, limited by the measurement frequency and the sample size. It is calculated as:

$$\sigma_y^2(\tau) = \frac{1}{2} E\left((\bar{y}_{n+1} - \bar{y}_n)^2\right). \tag{5.1}$$

The data $y(t)$ is divided into n parts with n being a multiple of the measurement frequency. τ is the time length of each part. For all parts the mean value, and its deviation to the subsequent mean value, is determined. For each τ the expectation value E of the deviations is determined. Calculating the square root of the Allan variance gives the Allan deviation.

[4]The voltmeter used for this measurement is a Fluke 8846A.

2022 JINST 17 P06003

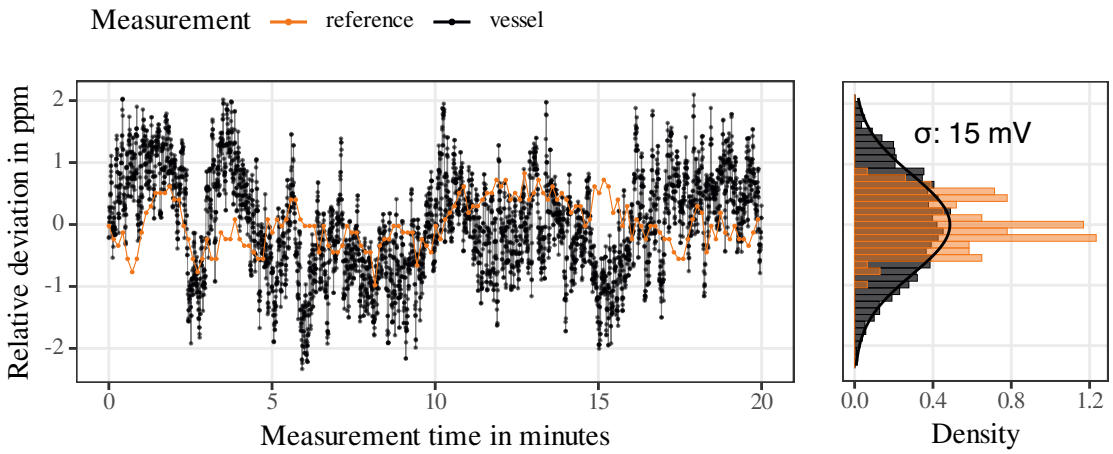

Figure 16. *Fast voltage measurement.* The relative deviation of the reference potential as measured by the high voltage divider K35 is plotted in orange. The relative deviation of the vessel potential (at −18.6 kV) is plotted in black. The vessel potential is the sum of reference potential and difference potential.

For all three measurement methods, the Allan deviation is determined and plotted in figure 17. Comparing the measurement with the fast-measurement system and the ripple probe measurement one can see that the sensitivity of the fast-measurement system starts where the ripple probe's sensitivity fades. It is important to note that the instability increases for longer time scales, so the part measured by the ripple probe but not seen by the fast-measurement system is more stable. This is again true for frequencies not measured by the high-voltage divider K35, here the fast-measurement system shows an overall higher stability. The fast instabilities measured by the fast-measurement system, are far below our stability requirement. It is very well justified to have only the K35 measurement in place for continuous monitoring of the high voltage during neutrino mass measurements at KATRIN.

The measurements with the fast-measurement system and with the high-voltage divider K35 were both performed without the DC drift correction. The yellow curve in figure 17 shows the performance with the DC drift correction. The DC drift correction removes the drifts on longer time scales (> minutes), as already visible in figure 15.

6 Conclusion

A custom-designed high-voltage system for KATRIN's main spectrometer has been developed, implemented, and tested. It outperforms the accuracy requirements set in the design report [1] by providing a retarding high voltage with sub-ppm precision and ppm-trueness at timescales from microseconds up to several weeks.

This solution comprises a nested regulation structure starting with a non-attenuating ripple pickup for low-noise smoothing of the retarding voltage, employing a medium-accuracy auxiliary voltage divider for intermediate timescales (seconds) and a drift compensation. The regulation structure deals with significant interference sources imposed by the large spectrometer vessel, which is not only openly exposed to external electromagnetic influence but also hosts its own isolated AC power net. Fast fine control of the high voltage is obtained by a ballast triode shunt

2022 JINST 17 P06003

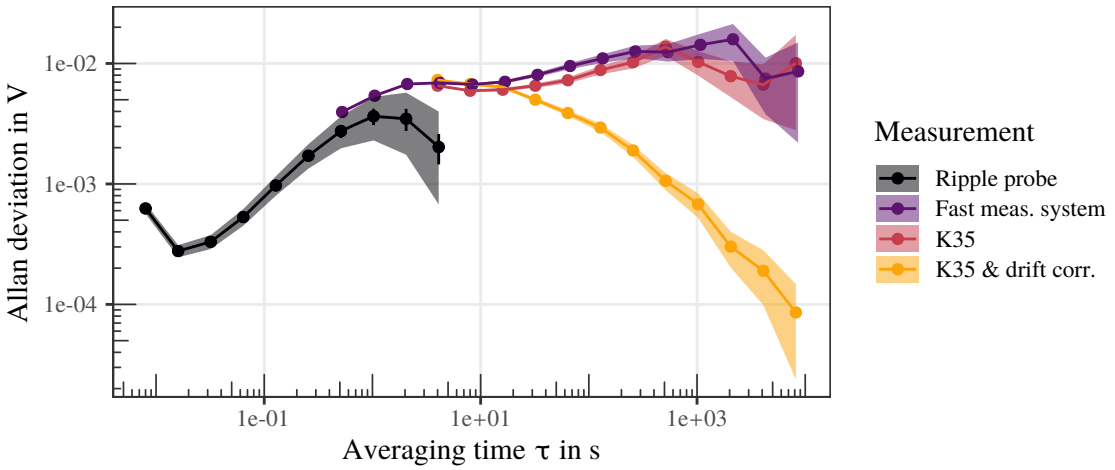

Figure 17. *Allan deviation.* At a retarding potential of −18.6 kV the Allan deviation was determined for different measurement types. In all four cases, the post-regulation system was active without the DC drift correction. Except for the data shown in yellow, here the DC drift correction was active. The readout rate for the K35 voltmeter is 1/2 Hz and for the fast-measurement system 3 Hz. For all three the sample interval spans over 11 h. For the ripple probe, the avarage Allan deviation over 1004 traces is plotted. Each trace is taken at a sample rate of 250 Hz over 33 s, the ripple probe is not limited to 250 Hz (cf. 5.1).

regulator seen before in 1960s color TV sets. For the drift compensation, precision high-voltage dividers are in place, allowing one to trace the retarding voltage back to absolute metrological standards. The performance of the system was proven with independent methods, including ^{83m}Kr conversion electron measurements.

During ongoing neutrino mass measurement campaigns [10, 26] the high-voltage regulation system is continuously running and providing a retarding potential with ppm-accuracy. Up to now, and also to be expected for future campaigns, the systematic uncertainty of the retarding potential is negligible for the neutrino mass measurement of KATRIN.

Acknowledgments

The authors would like to express their gratitude to the members of the KATRIN collaboration, in particular G. Franklin and L. Thorne for the GridSynch box, and the slow control and detector run control task group, with special thanks to F. Fränkle and T. Höhn. We acknowledge the support of Helmholtz Association (HGF), Ministry for Education and Research BMBF (05A20PMA), Deutsche Forschungsgemeinschaft DFG (Research Training Group GRK 2149) and the Department of Energy through grants DE-FG02-97ER41020, DE-FG02-94ER40818, DE-SC0004036, DE-FG02-97ER41033, DE-FG02-97ER41041, DE-SC0011091 and DE-SC0019304 and the Federal Prime Agreement DE-AC02-05CH11231 in the United States.

References

[1] KATRIN collaboration, *KATRIN design report*, Tech. Rep., Forschungszentrum Karlsruhe (2005), FZKA 7090 [DOI: 10.5445/IR/270060419].

2022 JINST 17 P06003

[2] KATRIN collaboration, *The design, construction, and commissioning of the KATRIN experiment*, 2021 *JINST* **16** T08015 [arXiv:2103.04755].

[3] A. Marsteller, B. Bornschein, L. Bornschein, G. Drexlin, F. Friedel, R. Gehring et al., *Neutral tritium gas reduction in the katrin differential pumping sections*, *Vacuum* **184** (2021) 109979.

[4] G. Beamson, H.Q. Porter and D.W. Turner, *The collimating and magnifying properties of a superconducting field photoelectron spectrometer*, *J. Phys. E* **13** (1980) 64.

[5] V.M. Lobashev and P.E. Spivak, *A method for measuring the anti-electron-neutrino rest mass*, *Nucl. Instrum. Meth. A* **240** (1985) 305.

[6] A. Picard, H. Backe, H. Barth, J. Bonn, B. Degen, T. Edling et al., *A solenoid retarding spectrometer with high resolution and transmission for keV electrons*, *Nucl. Instrum. Meth. B* **63** (1992) 345.

[7] J.F. Amsbaugh et al., *Focal-plane detector system for the KATRIN experiment*, *Nucl. Instrum. Meth. A* **778** (2015) 40 [arXiv:1404.2925].

[8] T. Thümmler, R. Marx and C. Weinheimer, *Precision high voltage divider for the KATRIN experiment*, *New J. Phys.* **11** (2009) 103007 [arXiv:0908.1523].

[9] S. Bauer, R. Berendes, F. Hochschulz, H.W. Ortjohann, S. Rosendahl, T. Thümmler et al., *Next generation KATRIN high precision voltage divider for voltages up to 65kV*, 2013 *JINST* **8** P10026 [arXiv:1309.4955].

[10] KATRIN collaboration, *Direct neutrino-mass measurement with sub-electronvolt sensitivity*, *Nature Phys.* **18** (2022) 160 [arXiv:2105.08533].

[11] D. Furse et al., *Kassiopeia: A Modern, Extensible C++ Particle Tracking Package*, *New J. Phys.* **19** (2017) 053012 [arXiv:1612.00262].

[12] N. Steinbrink, V. Hannen, E.L. Martin, R.G.H. Robertson, M. Zacher and C. Weinheimer, *Neutrino mass sensitivity by MAC-E-Filter based time-of-flight spectroscopy with the example of KATRIN*, *New J. Phys.* **15** (2013) 113020 [arXiv:1308.0532].

[13] A. Fulst, A. Lokhov, M. Fedkevych, N. Steinbrink and C. Weinheimer, *Time-Focusing Time-of-Flight, a new method to turn a MAC-E-filter into a quasi-differential spectrometer*, *Eur. Phys. J. C* **80** (2020) 956 [arXiv:2007.01020].

[14] R.G.H. Robertson and D.A. Knapp, *Direct Measurements of Neutrino Mass*, *Ann. Rev. Nucl. Part. Sci.* **38** (1988) 185.

[15] *Accuracy (trueness and precision) of measurement methods and results*, Standard 5725-1, International Organization for Standardization, Geneva, CH (1994).

[16] O. Rest, D. Winzen, S. Bauer, R. Berendes, J. Meisner, T. Thümmler et al., *A novel ppm-precise absolute calibration method for precision high-voltage dividers*, *Metrologia* **56** (2019) 045007.

[17] M. Arenz et al., *Calibration of high voltages at the ppm level by the difference of ^{83m}Kr conversion electron lines at the KATRIN experiment*, *Eur. Phys. J. C* **78** (2018) 368 [arXiv:1802.05227].

[18] KATRIN collaboration, *Analysis methods for the first KATRIN neutrino-mass measurement*, *Phys. Rev. D* **104** (2021) 012005 [arXiv:2101.05253].

[19] KATRIN collaboration, *First transmission of electrons and ions through the KATRIN beamline*, 2018 *JINST* **13** P04020 [arXiv:1802.04167].

[20] M. Kraus, *Energy-scale systematics at the KATRIN main spectrometer*, Ph.D. thesis, Karlsruher Institut für Technologie (2016) [DOI: 10.5445/IR/1000054447].

2022 JINST 17 P06003

[21] O. Rest, *Precision high voltage at the KATRIN experiment and new methods for an absolute calibration at ppm-level for high-voltage dividers*, Ph.D. thesis, Westfälische Wilhelms-Universität Münster (2019).

[22] D. Vénos, J. Sentkerestiová, O. Dragoun, M. Slezák, M. Ryšavý and A. Špalek, *Properties of 83mKr conversion electrons and their use in the KATRIN experiment*, 2018 *JINST* **13** T02012.

[23] K. Altenmüller et al., *High-resolution spectroscopy of gaseous ^{83m}Kr conversion electrons with the KATRIN experiment*, *J. Phys. G* **47** (2020) 065002 [arXiv:1903.06452].

[24] A. Fulst, *A Novel Quasi-Differential Method for MAC-E Filters and Determination and Control of the Electric Potentials of the KATRIN Experiment with a Stabilized Condensed Krypton Source and a UV Illumination System*, Ph.D. thesis, Westfälische Wilhelms-Universität Münster (2020).

[25] D. Allan, *Statistics of atomic frequency standards*, *Proc. IEEE* **54** (1966) 221.

[26] KATRIN collaboration, *Improved Upper Limit on the Neutrino Mass from a Direct Kinematic Method by KATRIN*, *Phys. Rev. Lett.* **123** (2019) 221802 [arXiv:1909.06048].

2022 JINST 17 P06003